Philosophical Magazine
Publication details, including instructions for authors and subscription information:
http://www.tandfonline.com/loi/tphm20

Comparison of the deformation behaviour of commercially pure titanium and Ti–5Al–2.5Sn(wt.%) at 296 and 728 K

H. Li [a], D.E. Mason [b], Y. Yang [a], T.R. Bieler [a], M.A. Crimp [a] & C.J. Boehlert [a]

[a] Department of Chemical Engineering and Materials Science, Michigan State University, East Lansing, MI, 48824, USA

[b] Department of Mathematics and Computer Science, Albion College, Albion, MI, 49224, USA

Published online: 02 May 2013.

To cite this article: H. Li, D.E. Mason, Y. Yang, T.R. Bieler, M.A. Crimp & C.J. Boehlert (2013) Comparison of the deformation behaviour of commercially pure titanium and Ti–5Al–2.5Sn(wt.%) at 296 and 728K, Philosophical Magazine, 93:21, 2875-2895, DOI: 10.1080/14786435.2013.791752

To link to this article: http://dx.doi.org/10.1080/14786435.2013.791752

Philosophical Magazine, 2013
Vol. 93, No. 21, 2875–2895, http://dx.doi.org/10.1080/14786435.2013.791752

Comparison of the deformation behaviour of commercially pure titanium and Ti–5Al–2.5Sn(wt.%) at 296 and 728 K

H. Li[a], D.E. Mason[b], Y. Yang[a], T.R. Bieler[a], M.A. Crimp[a] and C.J. Boehlert[a]

[a]*Department of Chemical Engineering and Materials Science, Michigan State University, East Lansing, MI 48824, USA;* [b]*Department of Mathematics and Computer Science, Albion College, Albion, MI 49224, USA*

(*Received 17 February 2013; final version received 22 March 2013*)

The tension and tensile-creep deformation behaviours of a fully-α phase commercially pure (CP) Ti and a near-α Ti–5Al–2.5Sn(wt.%) alloy deformed *in situ* inside a scanning electron microscope were compared. Tensile tests were performed at 296 and 728 K, while tensile-creep tests were performed at 728 K. The yield stress of CP Ti decreased dramatically with increasing temperature. In contrast, temperature had much smaller effect on the yield stress of Ti–5Al–2.5Sn(wt.%). Electron backscattered diffraction was performed both before and after the deformation, and slip trace analysis was used to determine the active slip and twinning systems, as well as the associated global stress state Schmid factors. In tension tests of CP Ti, prismatic slip was the most likely slip system to be activated when the Schmid factor exceeded 0.4. Prismatic slip was observed over the largest Schmid factor range, indicating that the local stress tensor varies significantly from the global stress state of uniaxial tension. The basal slip activity in Ti–5Al–2.5Sn(wt.%) was observed in a larger faction of grains than in CP Ti. Pyramidal $\langle c+a \rangle$ slip was more prevalent in CP Ti. Although twinning was an active deformation mode in tension tests of the CP Ti, it was rare in Ti–5Al–2.5Sn(wt.%). During creep, dislocation slip was the primary apparent deformation mechanism in CP Ti, while evidence for dislocation slip was much less apparent in Ti–5Al–2.5Sn(wt.%), where grain boundary sliding was dominant. A robust statistical analysis was carried out to assess the significance of the comparative activity of the different slip systems under the variety of experimental conditions examined.

Keywords: titanium; tension; creep; Schmid factor; deformation behaviour

1. Introduction

Due to the important commercial structural applications of titanium (Ti) and Ti alloys, the plastic deformation behaviour of the hexagonal α-phase Ti has been extensively studied [1–6]. At room temperature (RT), $\{1\,0\,\bar{1}\,0\}[1\,1\,\bar{2}\,0]$ prismatic slip is the most active deformation mode in α-phase Ti [4–5]. Other than prismatic slip, there are three other dislocation slip systems: $\{0\,0\,0\,1\}\ \langle 1\,\bar{2}\,1\,0\rangle$ basal slip, $\{1\,0\,\bar{1}\,0\}\ \langle 1\ \bar{2}\,1\,0\rangle$ pyramidal $\langle a\rangle$ slip, and $\{1\,0\,\bar{1}\,0\}\ \langle 2\ \bar{1}\ \bar{1}\,3\rangle$ first-order pyramidal $\langle c+a\rangle$ slip that can be activated

*Corresponding author. Email: boehlert@egr.msu.edu

provided that the resolved shear stress is high enough. There are also four twinning systems in α-phase Ti [6], $\{1\,0\,\bar{1}\,2\}\langle\bar{1}\,0\,1\,1\rangle$ T1 tensile twinning, $\{1\,1\,\bar{2}\,1\}\langle\bar{1}\ \bar{1}\,2\,6\rangle$ T2 tensile twinning, $\{1\,1\ \bar{2}\,2\}\langle 1\,1\ \bar{2}\ \bar{3}\rangle$ C1 compressive twinning and $\{1\,0\ \bar{1}\,0\}\langle 1\,0\ \bar{1}\,2\rangle$ C2 compressive twinning. When the maximum principal stress direction is oriented close to the *c-axis*, either $\langle c+a\rangle$ slip and/or twinning systems will have higher Schmid factors, i. e. higher resolved shear stress, than basal and prismatic slip systems, which allows easier twinning or pyramidal $\langle c+a\rangle$ slip activation. For commercially pure (CP) Ti, the most commonly observed twinning system at RT is $\{1\,0\,\bar{1}\,2\}\ \langle\bar{1}\,0\,1\,1\rangle$ (T1 tensile twinning).

The activation of each deformation mode in CP Ti has been studied over a wide temperature range [3,7–9]. Although values for the critical resolved shear stresses (CRSS) measured at RT vary significantly; there is general agreement that prismatic slip is significantly easier to activate than other modes, and that basal slip is more easily activated than pyramidal $\langle c+a\rangle$ slip [3,7–9]. Conrad [8] and Akhtar and Teghtsoonian [9] both found that this trend continued up to 1100 K.

Although prismatic slip remains the most easily activated slip system in CP Ti, basal slip tends to be more easily activated in the near-α and α + β alloys [4,10,11]. Studies have shown that both Al and Sn additions result in an increase of the *c*/*a* ratio [12–13] towards the ideal *c*/*a* of 1.633 [14]. Thus, a more close-packed basal plane is expected in the alloys containing Al and Sn compared to CP Ti, which can help account for more favourable basal slip with increasing Al and Sn.

Temperature and microstructure affect the twinning activity [3,8,11,15–18]. Extensive twin activity was found during RT four-point bending of polycrystalline CP Ti [3,15] and 78 K tensile tests of single crystal CP Ti [16], but a lack of twinning in single crystal of CP Ti has been reported above 500 K [8,16] and up to temperature as high as 1073 K [17]. Williams et al. [11] showed that the twinning activity decreased with increasing temperature for single crystals of α Ti–Al alloys ranging from Ti–1.4Al to Ti–6.6Al. They also showed that twinning was less active with increasing Al content. Twinning has been observed at 1088 K in polycrystalline CP Ti by McHargure and Hammond [18]. Thus, it appears that at elevated temperatures, twinning is more likely in polycrystalline microstructures than single crystals.

Although there have been a large number of studies [1–5,6–11,14–17,18–21] on the active deformation modes in Ti and Ti alloys, most of these have been conducted on single crystals, so a systematic comparison between the deformation behaviour of polycrystalline CP Ti and Ti alloys is lacking. In the present study, polycrystalline fully-α CP Ti and near-α Ti–5Al–2.5Sn(wt.%)[1] specimens were deformed in tension at 296 and 728 K to provide a sample of grains large enough to assess the relative activation of the different deformation modes under different environmental conditions. These modes have been identified using electron backscattered diffraction (EBSD) based trace analysis. The active deformation mechanisms have been compared at both low and high temperature using identical experiments. In addition, both polycrystalline fully-α CP Ti and near-α Ti–5Al–2.5Sn specimens were deformed in tensile creep at 728 K in order to identify the differences in deformation characteristics with high and low stress and a different strain rate. Collected data were analysed using multivariate parametric statistics to determine the likelihood that the observed differences and similarities in activation prevalence were indicative of an underlying systemic variation.

2. Experimental details

The CP Ti examined in this study was provided by the National Energy Technology Laboratory in Albany, Oregon, and was made using the Armstrong process to produce the original sponge that was compacted into an electrode and melted. The resulting 150 mm diameter ingot had been triple vacuum arc remelted, and then upset forged, forge flattened and squared before rolling. The forging steps were performed above the beta transus, while the rolling passes were performed at lower temperatures. The Ti–5Al–2.5Sn alloy was provided by Pratt & Whitney, Rocketdyne and had been forged in the upper half of the $\alpha+\beta$ phase field. The forged material had been given a 1227 K recrystallization anneal for 1 h followed by air cooling, and a subsequent vacuum anneal at 1033 K for 4 h was used to reduce the hydrogen content.

Flat dog bone samples, containing a 10 mm gage length, were machined and mechanically polished. The final polish involved a solution of five parts 0.06 μm colloidal silica and one part 30% hydrogen peroxide by volume. Prior to deformation, EBSD mapping was conducted using a Camscan 44FE field emission gun scanning electron microscope (SEM) (Cambridge, UK) equipped with an EDAX-TSL (Mahwah, NJ, USA) EBSD system. Backscattered electron (BSE) and/or secondary electron (SE) photomicrographs were acquired both before and after deformation. Phase volume percents were determined using ImageJ image analysis software on BSE SEM photomicrographs. The equiaxed grain size was measured using the line-intercept method [22].

296 and 728 K tensile experiments were performed inside a Carl Zeiss EVO LS25 SEM. A constant displacement rate of 0.004 mm/s was used to control the tensile tests, corresponding to a strain rate of approximately $10^{-3}s^{-1}$. Load and displacement were recorded throughout the experiments using MTESTW data acquisition and control software (Admet, Inc., Norwood, MA, USA). For the 728 K tensile experiments, the samples were heated to the desired temperature and maintained at that temperature for at least 30 min prior to deformation to reduce thermal gradients. The temperature was monitored using a thermocouple spot-welded to the side of the gage sections. The experiments were paused at various stages to collect BSE and/or SE images. Local strains were estimated by measuring the relative displacements of obvious microstructural features on SEM images acquired before and after deformation. The strains reported in this paper are local strains. None of the samples were taken to failure. One experiment was performed for each material at each temperature investigated with the exception of the RT CP Ti experiment which was performed in duplicate. Some of the results from the tensile experiments of the Ti–5Al–2.5Sn were reported in [21].

In addition, tensile-creep experiments were performed on both materials at 728 K inside a SEM as described in [21]. The applied creep stresses used for CP Ti (45 MPa) and Ti–5Al–2.5Sn (250 MPa) were 0.73 and 0.76 that of the yield stress, respectively.

The global Schmid factor was defined for each deformation system in each grain of interest based on the EBSD determined orientation and the assumption of a uniaxial tensile stress. The plane trace of each system on the sample surface was calculated by the cross product of the slip/twinning plane and the grain surface normal. As a first estimate, for the basal and pyramidal slip systems which have three slip directions on each plane, the slip direction with the highest global Schmid factor was assumed to be the active slip system associated with that particular slip trace. Thus, the different slip systems on basal and pyramidal planes were distinguished with this assumption. It is noted that the

experimentally-observed slip traces were always within two degrees of the chosen simulated plane trace of the deformation system. While this same approach was used to identify twins; this approach was confirmed by comparing the EBSD measured twin orientations with their parent orientations, as each type of twin has a unique misorientation angle and rotation axis with respect to the parent orientation. A more detailed description of this deformation analysis technique is provided elsewhere [15]. It is important to note that a minimum of 86 grains that exhibited obvious traces due to slip or twinning were characterized in tensile-tested specimens, with at least 120 instances of observed deformation systems in those grains. Multiple parallel slip lines were typically observed and counted as one active deformation system. It is noted that the observed slip traces were a result of dislocation motion. There are several reasons why some grains may not develop observable slip lines, including the Burgers vectors were parallel to the sample surface, the slip was diffuse and was not constrained to well-defined slip bands, or the magnitude of slip was small and the slip bands were not well developed.

3. Results

3.1. *Microstructure*

Figure 1 shows characteristic SEM images of the as-received CP Ti and Ti–5Al–2.5Sn microstructures. The average hexagonal closed packed α grain size was 115 μm for CP Ti and 45 μm for Ti–5Al–2.5Sn. In Ti–5Al–2.5Sn, the body centered cubic (BCC) β phase (light color in Figure 1(b)) decorated some of the equiaxed α-phase grain boundaries. The volume fraction of β phase was less than 1%. Although the deformation behaviour of the β phase is not presented in this work, a description of the β-phase deformation behaviour and the α/β slip transfer is provided in reference [23].

Figure 2 shows the $\{0\,0\,0\,1\}$ and $\{1\,0\,\bar{1}\,0\}$ pole figures, as measured by EBSD, of six specimens prior to deformation; three for each material studied. These specimens were later tensile tested at either 296 or 728 K. CP Ti exhibited a weak fiber texture with an approximately 4 times random texture. The Ti–5Al–2.5Sn specimens lacked

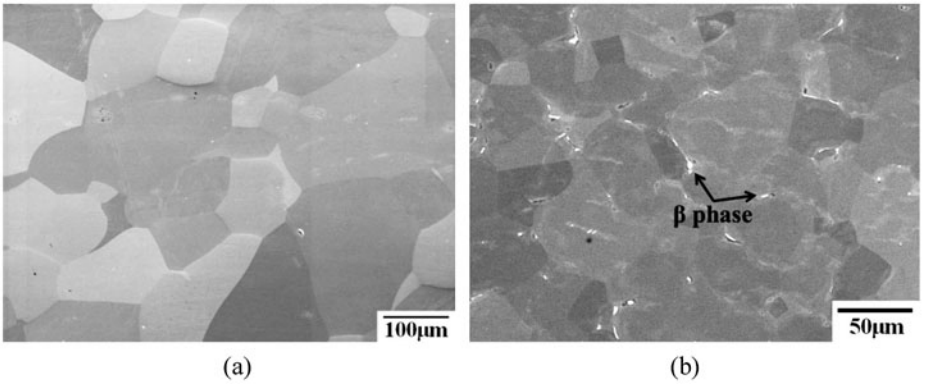

Figure 1. (a) SE SEM photomicrograph of the as-received CP Ti, (b) BSE SEM photomicrograph of the as-forged Ti–5Al–2.5Sn. The β phase (light phase) decorated the equiaxed α phase (dark phase) grain boundaries.

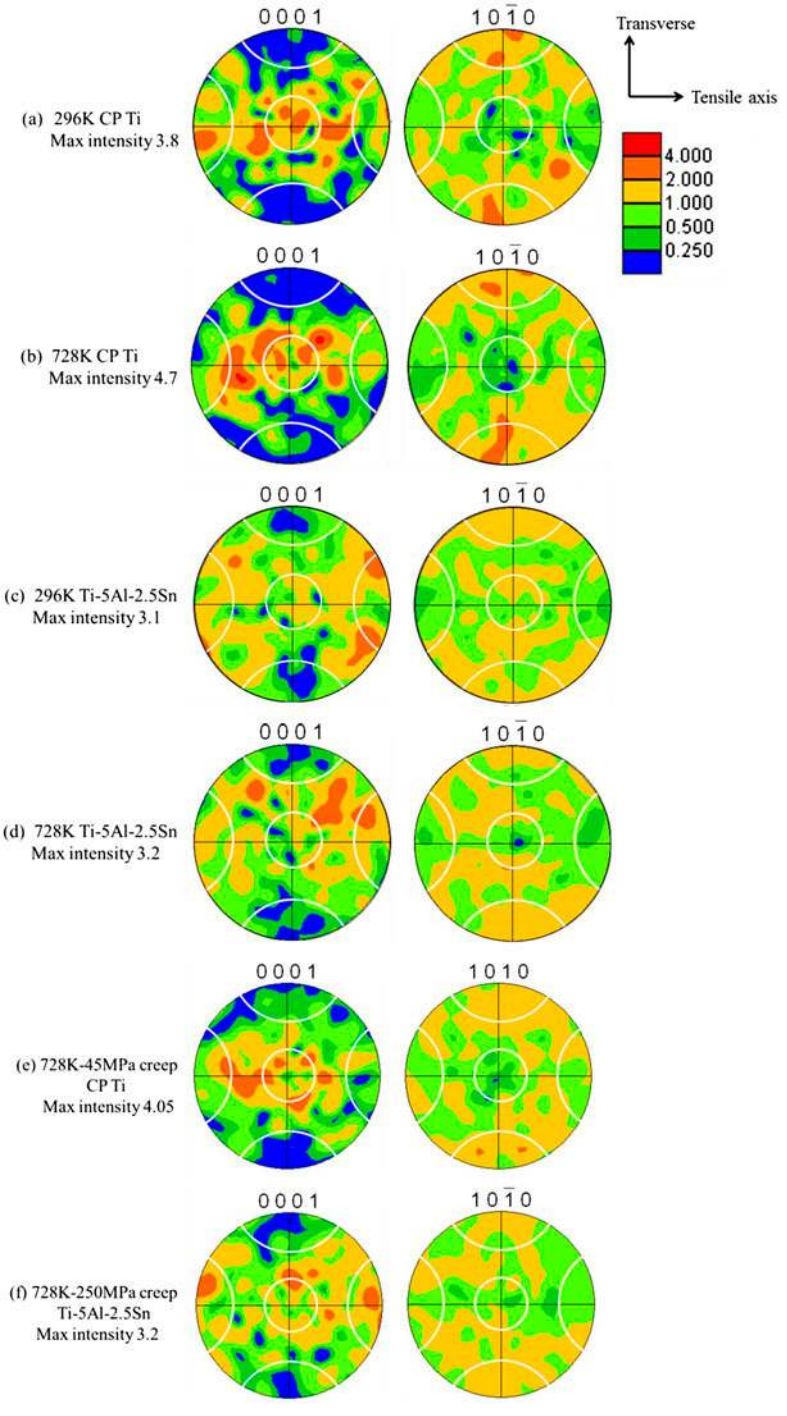

Figure 2. The $\{0\,0\,0\,1\}$ and $\{1\,0\,\bar{1}\,0\}$ pole figures with 30° cones along the major axes from (a) 296 K tension of CP Ti, (b) 728 K tension of CP Ti, (c) 296 K tension of Ti–5Al–2.5Sn, (d) 728 K tension of Ti–5Al–2.5Sn, (e) 728 K-45 MPa creep of CP Ti, and (f) 728 K-250 MPa creep of Ti–5Al–2.5Sn measured using EBSD. CP Ti specimens exhibited weak fiber texture and Ti–5Al–2.5Sn lacked any symmetric texture characteristics.

Table 1. Percentage of grains having a global Schmid factor of at least 0.4 for basal, prismatic, pyramidal ⟨a⟩, or pyramidal ⟨c + a⟩ slip before deformation.

Specimen	Basal (%)	Prismatic (%)	Pyramidal ⟨a⟩ (%)	Pyramidal ⟨c + a⟩ (%)
296 K tension of CP Ti	36	38	65	82
728 K tension of CP Ti	45	33	57	83
728 K-45 MPa creep of CP Ti	37	36	60	81
296 K tension of Ti–5Al–2.5Sn	45	31	57	82
728 K tension of Ti–5Al–2.5Sn	48	30	56	81
728 K-250 MPa creep of Ti–5Al–2.5Sn	39	38	63	81

any symmetric texture characteristics, and peaks were found at random orientations which were no stronger than 4 times random texture.

Table 1 lists the percentage of grains with global Schmid factors of at least 0.4 for basal, prismatic, pyramidal ⟨a⟩, and pyramidal ⟨c + a⟩ slip for each test condition evaluated. The pyramidal slip systems accounted for the highest percentages, however they also exhibited significantly greater CRSS values than basal and prismatic slip systems. The percentage of grains with global Schmid factors greater than 0.4 for basal slip ranged between 36 and 48%, with this percentage between 30 and 38% for prismatic slip.

3.2. *296 K tension behaviour of CP Ti*

Figure 3 shows the stress vs. displacement curve and the corresponding sequential SE SEM images taken from the same area of the specimen during the 296 K tensile test for CP Ti. Both slip and twinning surface traces were first observed at a stress level of 426 MPa, which was just below the global yield stress, ~440 MPa. Most of the slip traces were identified to be prismatic slip systems (indicated by red lines in Figure 3(c)) and their global Schmid factors ranged from 0.25 to 0.48. A larger number of twins and slip traces were observed at higher strain levels. T1 twins were the only type of twins observed. This is consistent with previous findings for RT deformed CP Ti [6]. Some grain boundary ledges developed during the deformation.

137 active deformation systems in 108 grains were identified in the two tensile tests performed at 296K. Data from one of the tests, where 104 active deformation systems were observed in 77 total grains, is shown in Figure 3(a) and Figure 4, where the y-axis represents the number of observations of a particular deformation system in a certain global Schmid factor range. The data analysis was focused on this specimen, although the results of the second specimen was not significantly different. More than 85% of the activated deformation systems observed in both specimens 108 grains exhibited global Schmid factors greater than 0.3. 11 basal, 87 prismatic, 10 pyramidal ⟨a⟩ and 16 pyramidal ⟨c + a⟩ slip systems were identified, along with 13 twinning systems. The majority of the active deformation systems were of prismatic slip, which was activated over almost the entire global Schmid factor range. Thus, prismatic slip was the dominant deformation mode at 296 K. Basal, pyramidal ⟨a⟩ and pyramidal ⟨c + a⟩ slip systems and twinning comprised only a small fraction of the observed deformation modes, and most of those were associated with global Schmid factors greater than 0.4.

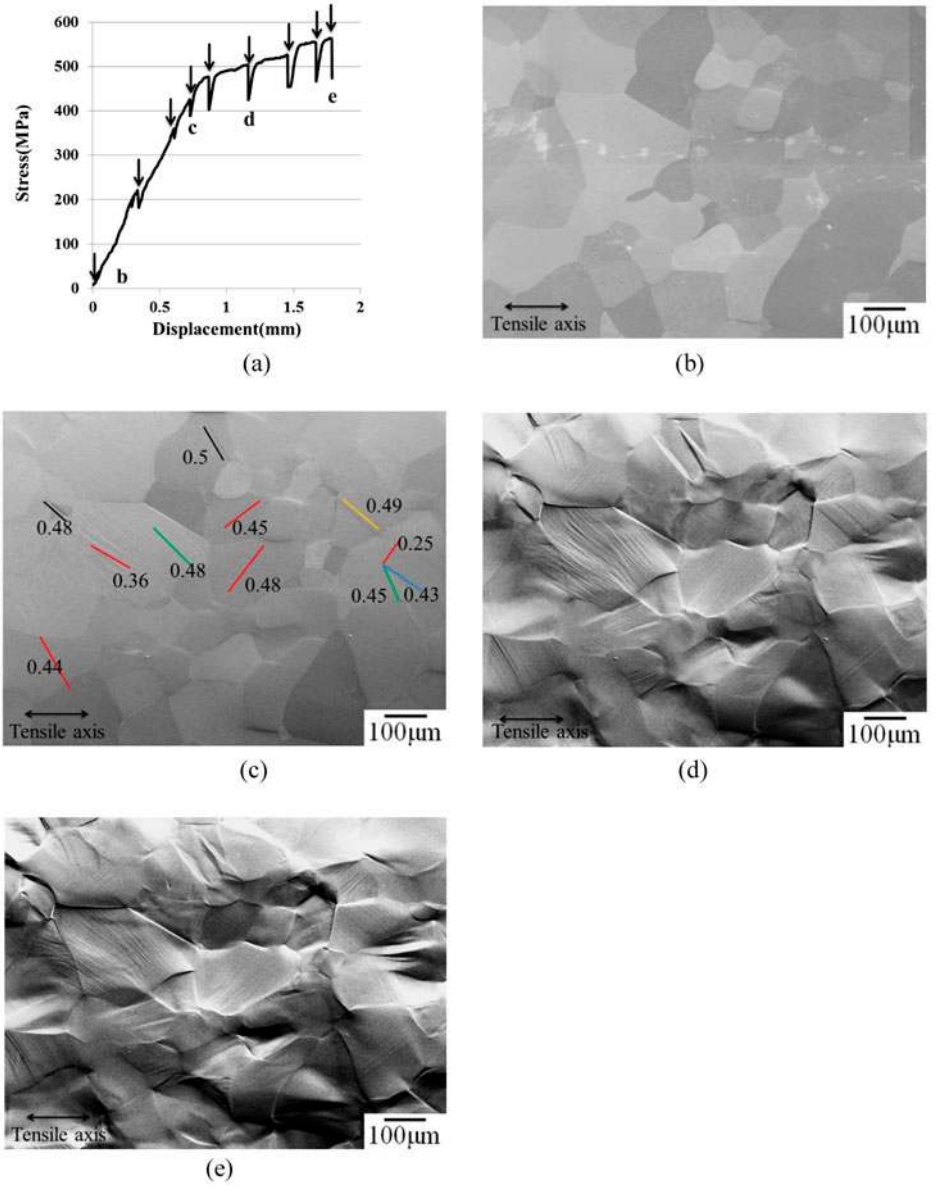

Figure 3. (colour online) (a) Engineering stress versus displacement curve of 296 K tension test of CP Ti, where arrows indicate when the test was interrupted for imaging and the letters b, c, d and e indicate when the SE SEM photomicrographs were acquired; (b) undeformed, (c) 426 MPa (when slip bands were first observed), (d) 504 MPa (~4% strain), and (e) 564 MPa (~8.4% strain). In (c), planes traces are color coded for prismatic slip (red), basal slip (blue), pyramidal ⟨a⟩ (green), pyramidal ⟨c + a⟩ (orange), and twin (black). The loading direction was horizontal, and the displacement values given in (a) were taken from the testing system, which included displacement in the grip regions.

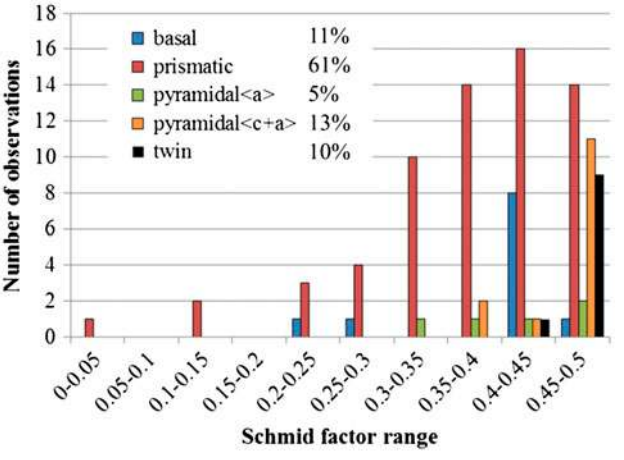

Figure 4. (colour online) A histogram of the global Schmid factor distribution of basal, prismatic, pyramidal ⟨c + a⟩, pyramidal ⟨a⟩ slip systems, and twinning for the 296 K CP Ti tensile experiment at ∼8.4% strain.

3.3. *728 K tension behaviour of CP Ti*

The stress vs. displacement curve for the CP Ti tensile sample deformed at 728 K and the correlated SE SEM images are shown in Figure 5. The yield stress (∼62 MPa) was significantly lower than the value observed at 296 K (∼440 MPa). Both twinning and slip traces were observed at a stress level of 64 MPa (∼2.4% strain). Most of the slip traces were identified as prismatic slip traces (highlighted by red lines in Figure 5), while much less basal (highlighted by blue lines in Figure 5), pyramidal ⟨c + a⟩ (highlighted by yellow lines in Figure 5), and twin (highlighted by black lines in Figure 5) traces were observed. Pyramidal ⟨a⟩ slip was not observed in this microstructure patch at ∼2.4% strain. At ∼11.2% strain, some grains exhibited multiple deformation systems. Some grain boundaries developed ledges, becoming evident at ∼4.3% strain.

Slip trace analysis was performed for 86 grains (including the subset shown in Figure 5), and 120 different deformation systems were identified. The histogram of the deformation modes with respect to the global Schmid factor is provided in Figure 6. About 79% of observed deformation systems were activated with relatively high global Schmid factors (greater than 0.3). The majority of the deformation systems were prismatic slip and a few prismatic slip systems were activated with low global Schmid factors (smaller than 0.1), which was similar to that observed for the 296 K CP Ti case. The activation of the other deformation systems occurred over a global Schmid factor range of 0.2–0.5.

3.4. *296 K tension behaviour of Ti–5Al–2.5Sn*

A microstructure patch from a tensile specimen deformed to ∼3.5% strain is shown in Figure 7. More information about this specimen can be found in [21]. 204 active

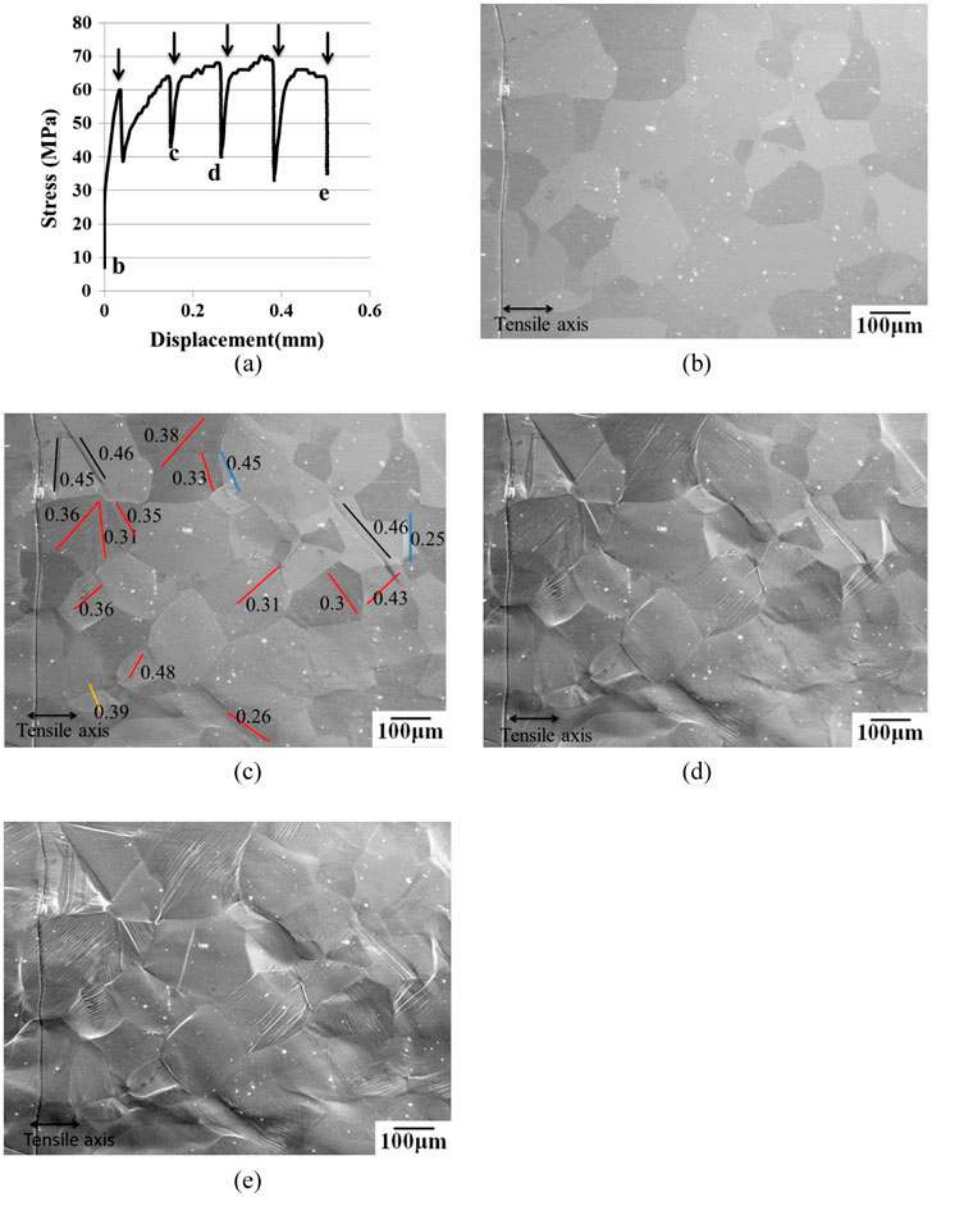

Figure 5. (colour online) (a) Engineering stress versus displacement curve of 728 K tension test of CP Ti, where arrows indicate when the test was interrupted for imaging and the letters b, c, d and e indicate when the SE SEM photomicrographs were acquired; (b) undeformed, (c) 64 MPa (when slip bands were first observed, ∼2.4% strain), (d) 67 MPa (∼4.3% strain), and (e) 66 MPa (∼11.2% strain). In (c), planes traces are color coded for prismatic slip (red), basal slip (blue), pyramidal ⟨a⟩ (green), pyramidal ⟨c + a⟩ (orange), and twin (black). The loading direction was horizontal, and the displacement values given in (a) were taken from the testing system, which included displacement in the grip regions. The intentional scratch on the left of the SE SEM images was used as a fiducial marker.

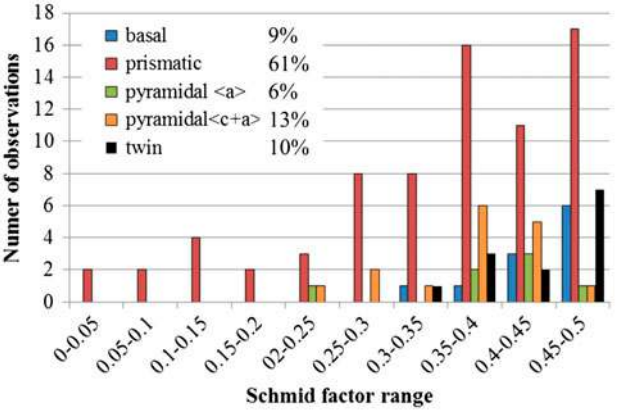

Figure 6. (colour online) A histogram of the global Schmid factor distribution of basal, prismatic, pyramidal ⟨c + a⟩, pyramidal ⟨a⟩ slip systems, and twinning for the 728 K CP Ti tensile experiment after ∼11.2% strain.

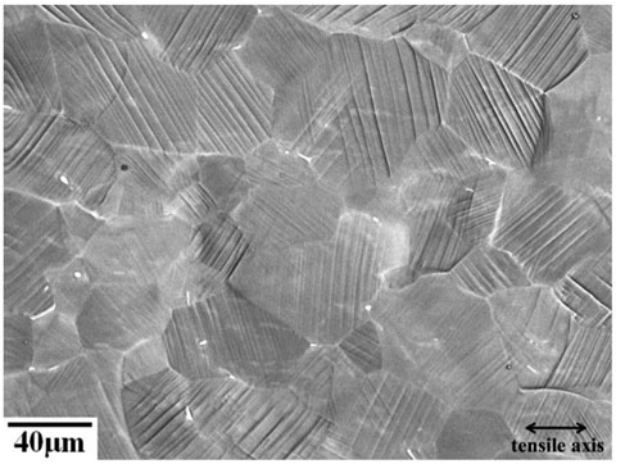

Figure 7. BSE SEM image showing a tensile deformed microstructural patch of Ti–5Al–2.5Sn at 296K with ∼3.5% strain.

deformation systems were identified in the 137 α grains, see Figure 8. Both basal and prismatic slip were the dominant deformation modes as they were associated with more than 90% of all the slip traces analysed (see Table 2). Pyramidal ⟨a⟩ and pyramidal ⟨c + a⟩ slip were typically observed with global Schmid factors greater than 0.4, suggesting that they were most likely activated to accommodate the local strain compatibility requirements. Only two twins were observed, indicating twinning was not a dominant deformation mode in Ti–5Al–2.5Sn at 296 K.

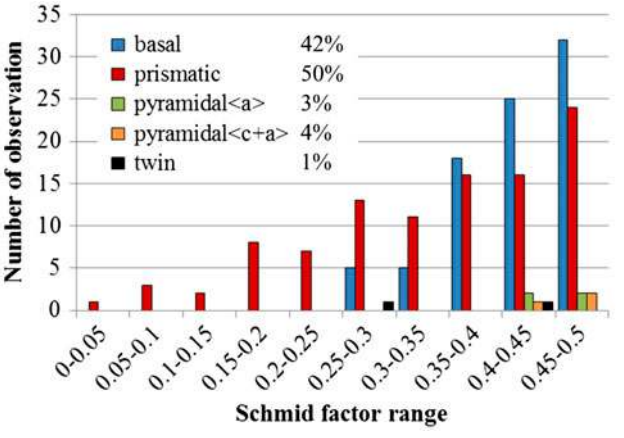

Figure 8. (colour online) A histogram of the global Schmid factor distribution of basal, prismatic, pyramidal ⟨c + a⟩, pyramidal ⟨a⟩ slip systems, and twinning for the 296 K Ti–5Al–2.5Sn tensile test after ∼3.5% strain.

Table 2. Distribution of the observed deformation systems in Ti–5Al–2.5Sn and CP Ti*.

Percentage of observations showing slip/twin system activity→ Test mode, materials (approx. strain)	Basal (%)	Prismatic (%)	Pyr ⟨a⟩ (%)	Pyr ⟨c+a⟩ (%)	Twin (%)
296 K tension of CP Ti (∼4%)	10	63	6	10	11
296 K tension of CP Ti (∼8.4%)	11	61	5	13	10
728 K tension of CP Ti (∼4.3%)	11	59	6	14	10
728 K tension of CP Ti (∼11.2%)	9	61	6	13	11
728 K-45 MPa creep of CP Ti (∼23.2%)	9	64	14	10	3
296 K tension of Ti–5Al–2.5Sn (∼3.5%)	42	50	3	4	1
728 K tension of Ti–5Al–2.5Sn (∼4.4%)	48	41	5	6	0
728 K tension of Ti–5Al–2.5Sn (∼9%)	42	47	5	6	0
728 K-250 MPa creep of Ti–5Al–2.5Sn (∼16.5%)	78	16	2	4	0

*Note: that if a deformation system was observed in a single grain, it was only counted once independent of the number of slip traces observed in that grain.

3.5. *728 K tension behaviour of Ti–5Al–2.5Sn*

A microstructure patch from a tensile specimen after ∼9% strain at 728K in tension is shown in Figure 9 (additional information can also be found in [21]). Wavy slip lines indicated the development of cross slip. 192 active slip systems were identified in the 121 α grains. Similar to the 296 K tensile deformation, both basal and prismatic slip were the main deformation modes, as shown in Figure 10. Pyramidal ⟨a⟩ and pyramidal ⟨c + a⟩ slip were observed to a much lesser extent compared with basal and prismatic slip. Unlike at 296 K, twinning was not observed at 728 K.

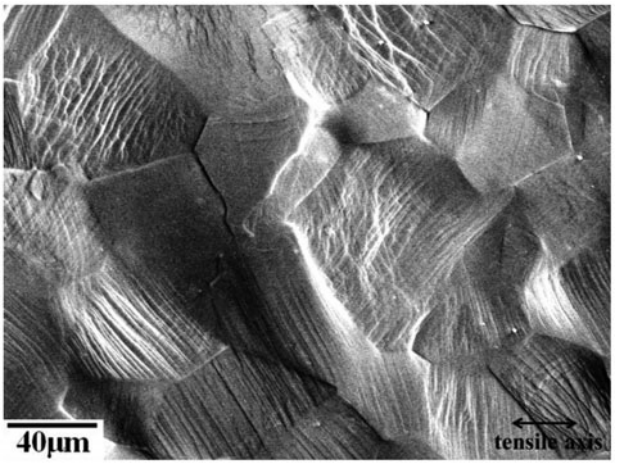

Figure 9. SE SEM image showing a tensile deformed microstructural patch of Ti–5Al–2.5Sn at 728 K with ∼9% strain.

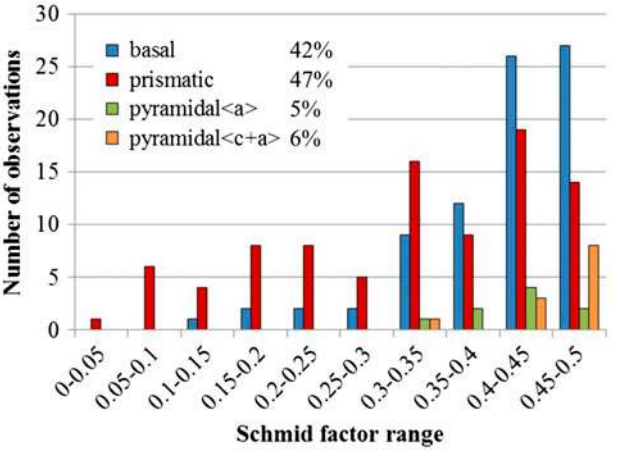

Figure 10. (colour online) A histogram of the global Schmid factor distribution of basal, prismatic, pyramidal ⟨c + a⟩, and pyramidal ⟨a⟩ slip systems for the 728K Ti–5Al–2.5Sn tensile experiment after ∼9% strain.

3.6. *728K-45MPa creep behaviour of CP Ti*

Figure 11 illustrates *in situ* SE SEM images acquired during the 728 K-45 MPa creep experiment. Grain boundary ledges were first observed at ∼1.4% strain, prior to any noticeable surface slip trace formation. At larger strain levels (see Figure 11(c) and (d)), almost all the grains developed dislocation slip. Slip traces analysis was performed for 107 grains and 162 deformation systems were identified, see Figure 12. Prismatic slip was the dominant deformation mode and it was activated over the largest global Schmid factor range ($0 \sim 0.5$). Basal, pyramidal ⟨a⟩, and pyramidal ⟨c + a⟩ slip systems were only observed with Schmid factors greater than 0.25 and comprised 9, 14 and 10% of

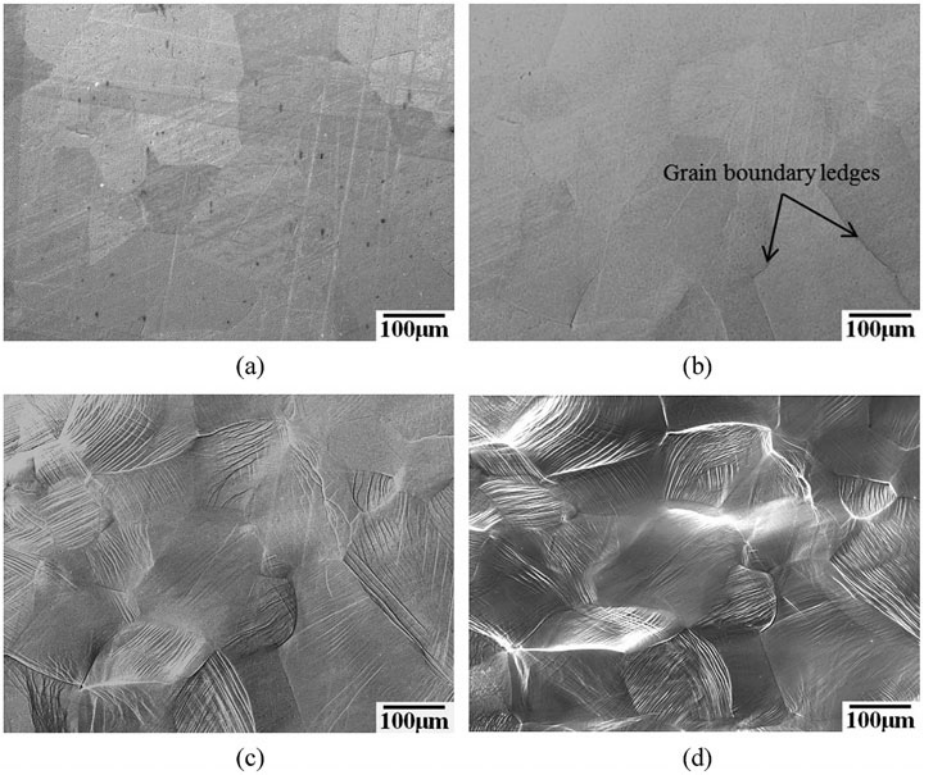

Figure 11. SE SEM photomicrographs taken for a given microstructure patch during the 728 K-45 MPa creep experiment in CP Ti. The approximate strain values were (a) 0%, (b) 1.4%, (c) 6%, and (d) 23.2%. The loading axis was horizontal.

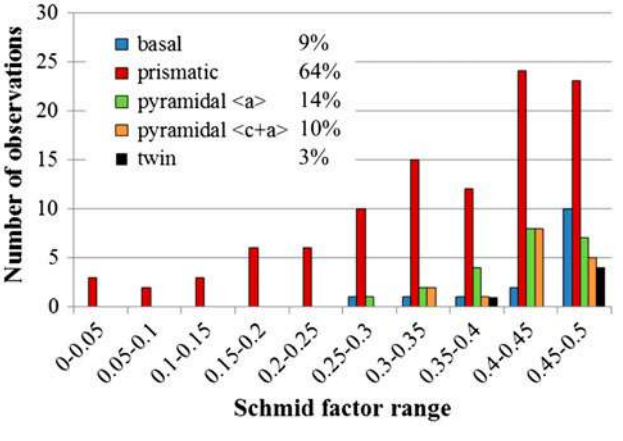

Figure 12. (colour online) A histogram of the global Schmid factor distribution of basal, prismatic, pyramidal ⟨c + a⟩, pyramidal ⟨a⟩ slip systems, and twinning for the 728 K-45 MPa CP Ti creep experiment at ∼23.2% strain.

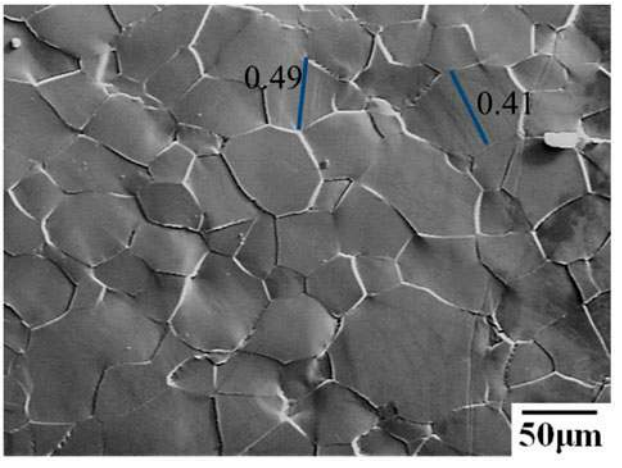

Figure 13. (colour online) SE SEM image showing a 728 K-250 MPa creep deformed microstructural patch of Ti–5Al–2.5Sn with ∼16.5% strain. Planes traces are color coded for basal slip (blue). The loading axis was horizontal.

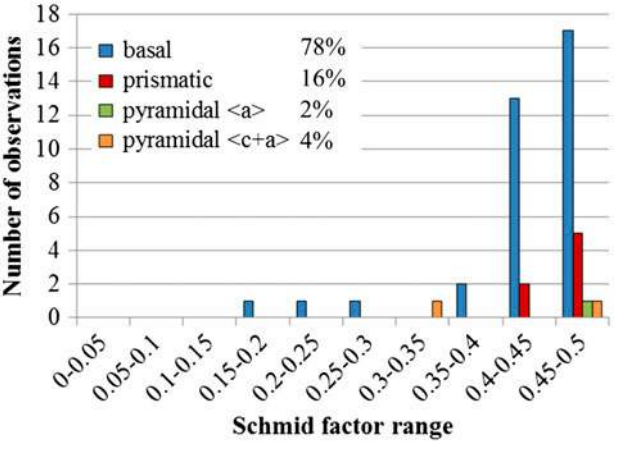

Figure 14. (colour online) A histogram of the global Schmid factor distribution of basal, prismatic, pyramidal ⟨a⟩, and pyramidal ⟨c + a⟩ slip systems for the 728 K-250 MPa Ti–5Al–2.5Sn creep experiment at ∼16.5% strain.

the total deformation systems, respectively (see Table 2). Twinning was also observed but to a much less extent; only 3% of the total deformation systems (see Table 2).

3.7. *728 K-250 MPa creep behavior of Ti–5Al–2.5Sn*

Figure 13 shows a SE SEM image of 728 K-250 MPa creep tested sample, which exhibited ∼16.5% strain (more information about this specimen can be found in ref [21]). During creep, grain boundary sliding (GBS) appeared to be an active deformation

mechanism, as evidenced by the observed grain boundary ledges (see Figure 13). Nearly all the grain boundaries formed ledges and only a few grains exhibited planar slip traces, suggesting that dislocation slip did not contribute to the strain as much as GBS. Figure 14 shows the slip trace analysis results. 35 out of 45 (78%) slip systems were identified to be basal slip. More than 90% of the activated basal slip systems exhibited relatively high global Schmid factors (>0.3). Prismatic, pyramidal $\langle a \rangle$ and pyramidal $\langle c + a \rangle$ systems only contributed 16, 2 and 4% of total deformation systems, respectively. No twining was observed.

4. Discussion

4.1. *Comparison of the tensile deformation behaviour*

The yield stress of CP Ti at 296 K was ~440 MPa, which decreased to ~62 MPa at 728 K. These values are similar to those obtained in grade 2 CP Ti [24]. For Ti–5Al–2.5Sn, the yield stress (~330 MPa) at 728 K was lower than that observed at 296 K (~660 MPa), and these values are consistent with previous measurements for this alloy [24].

Dislocation slip was the primary tensile deformation mechanism observed in the tensile tests. Table 2 lists the distribution of the deformation modes in both the materials at similar strain levels. In both CP Ti and Ti–5Al–2.5Sn, the percentage of observations for each deformation mode did not change significantly with temperature, indicating that the relative activity of the deformation modes is not sensitive to temperature. This hypothesis was assessed statistically as discussed in Section 4.4.

Prismatic slip was commonly observed in both materials and it was activated over a large global Schmid factor range at both 296 and 728 K (see Table 2). At least 41% of the total deformation systems were identified to be prismatic slip for each specimen. Compared to CP Ti, basal slip was more active in Ti–5Al–2.5Sn. At similar strain levels, the basal slip activity in Ti–5Al–2.5Sn was significantly greater than that in CP Ti at both 296 K (42% in Ti–5Al–2.5Sn vs. 10% in CP Ti) and 728 K (48% in Ti–5Al–2.5Sn vs. 11% in CP Ti) (see Table 2). These results are consistent with prior work that showed that the *c*/*a* ratio increased with increased Al and Sn content [12,13]. Higher Al contents make the basal slip planes more closely packed and are thus more favourable for slip. Therefore, basal slip activity increases relative to prismatic slip activity. Pyramidal $\langle a \rangle$ slip comprised less than 6% of the total deformation observations in both materials. Compared with Ti–5Al–2.5Sn, there was a slight increase in the relative extent of pyramidal $\langle c + a \rangle$ slip activity in CP Ti at both 296 and 728 K, suggesting that the CRSS of pyramidal $\langle c + a \rangle$ slip may be increased with alloying content. The probability that this hypothesis is correct will be quantified in Section 4.4.

Alloying suppressed mechanical twin formation. Twinning was only evident in few grains for Ti–5Al–2.5Sn deformed at 296 K. However, twinning was more frequently observed in CP Ti deformed at 296 and 728 K. The observation of the lack of deformation twinning in polycrystalline Ti–5Al–2.5Sn is therefore consistent with the observations of Williams et al. [11], who showed that twinning was inhibited by the ordering of Al in the α phase. However, in contrast to the observations of Williams et al. [11], who also showed that twin activity decreased with increasing temperature in Ti-Al single crystals, no obvious decrease in the relative twin activity with increasing temperature was observed in polycrystalline CP Ti.

Table 3. The ratio of the number of grains which exhibited basal or prismatic slip systems with Schmid factors >0.4 to the number of grains with the potential to exhibit that type of slip.

Test mode/material/approx. strain (%)	Basal (%)	Prismatic (%)
296 K tension CP Ti (4)	7/23 = 30	24/27 = 89
728 K tension CP Ti (11.2)	9/38 = 24	26/29 = 90
296 K tension Ti–5Al–2.5Sn (3.5)	60/68 = 88	39/39 = 100
728 K tension Ti–5Al–2.5Sn (9)	54/58 = 93	33/36 = 92

4.2. *Correlation of the global Schmid factor with the observed tensile deformation mode*

Although the local stress state can vary between individual grains and within grains due to stress concentrations, inhomogeneities, etc., the Schmid factor is an important parameter that is typically correlated with the activation of a particular deformation mode. Both basal and prismatic slip systems were the main deformation modes observed in this study. Table 3 shows the ratio of the number of grains that exhibited either basal or prismatic slip to the total number of grains with the potential to exhibit that type of slip. Only grains with global Schmid factors greater than 0.4 were considered in this analysis. The higher the ratio, the greater the likelihood that the global Schmid factor could be used reliably to predict the slip system activated. The temperature did not significantly affect the ratios for either material. The ratios, however, varied with material. For Ti–5Al–2.5Sn, the ratios were high for both basal and prismatic slip, indicating that both basal and prismatic slip systems with high global Schmid factors tended to be activated. A similar situation was observed for prismatic slip in CP Ti. However, this was not the case for basal slip in CP Ti, where less than 30% of those systems with high global Schmid factors actually exhibited basal slip at both 296 and 728 K. Those grains which exhibited global Schmid factors greater than 0.4 for basal slip, yet did not exhibit basal slip, tended to exhibit prismatic slip even though the global Schmid factors for prismatic slip were below 0.4. Thus, the results strongly support that prismatic slip is the preferred deformation mode in CP Ti.

The activation of slip systems with relatively low Schmid factor suggests that the local stress state can vary from the global stress tensor. If the global stress was realized in each grain, then all the same type of slip systems with equivalent Schmid factors would activate simultaneously at a given stress level. Analysis of the images where slip traces were first observed in each specimen, including (Figure 3(c) and Figure 5(c)), indicates this was not the case. The factor most likely responsible for this is the heterogeneity of the local stress tensor, which has been demonstrated in crystal plasticity computational simulations of microstructural patches [3,25–29]. In the heterogeneous deformation caused by differential deformation processes in adjacent grains, the variation in local strains affects the local stress tensor. While slip systems with high Schmid factors are observed more often, the presence of the observed slip systems with low global Schmid factors is an indirect indicator of the heterogeneous stress states and the ease of nucleation of slip systems that can accommodate required geometric changes [3,25–29]. The fact that prismatic slip shows a much wider spread suggests that nucleation of prismatic slip at grain boundaries may be easier than basal slip.

4.3. *Comparison of the 728 K tensile and tensile-creep deformation behavior*

During the elevated temperature tensile and tensile-creep tests, the relative activity of dislocation slip and GBS varied with testing modes and materials. During 728 K-250 MPa creep of Ti–5Al–2.5Sn, GBS appeared to be the major deformation mode rather than dislocation slip. Although the ratio of the applied creep stress to the yield stress was similar in CP Ti (0.73) and Ti–5Al–2.5Sn (0.76), dislocation slip, rather than GBS, was the primary deformation mode in 728 K-45 MPa CP Ti creep. It has been reported that finer grain sizes enhance GBS [30–32]. Thus, the deformation mechanism difference between CP Ti and Ti–5Al–2.5Sn during creep may be partially explained by the grain size difference between CP Ti (~115 μm) and Ti–5Al–2.5Sn (~45 μm). During the 728 K-250 MPa creep test of Ti–5Al–2.5Sn, only ~10% of the total grains exhibited slip traces, where 78% of deformation systems were for basal slip, and prismatic slip only comprised 16% (see Table 2). In contrast, for the 728 K tensile test of Ti–5Al–2.5Sn, ~94% of the total grains exhibited slip traces and the activation percentages of basal and prismatic slip were almost equivalent (see Table 2). Thus, GBS was the primary deformation mechanism in the 728 K-250 MPa creep test of Ti–5Al–2.5Sn and when slip occurred, basal slip was the preferred system. In CP Ti, however, the percentages of active deformation systems for basal and prismatic slip were similar in both 728 K tensile and 728 K-45 MPa creep tests (see Table 2). Thus, dislocation slip was the dominant deformation mechanism in both the tensile and tensile-creep tests of this material. The relatively likelihood of the slip activity in tension and tension creep is assessed in Section 4.4.

4.4. *Statistical analysis*

The data presented above suggest a number of different trends in the activation of the different deformation systems as a function of the different test conditions. The large number of observations allows a more robust parametric statistical analysis to be carried out, which is presented in this section. All statistical analysis was performed using original code written in *Mathematica*.

When comparing different deformation systems and their observed prevalence across all the experiments, it is important to first test that any variation in the relative sample frequency was the result of an underlying systemic difference and not simply data noise (i.e. test of homogeneity) [33]. One-way analysis of variance determined that, across all experiments, the data supported rejecting the hypothesis that all deformation systems were equally likely to be observed in a given material. These tests were conducted using both Tukey and Bonferroni methods at a 0.01 level of significance and yielded similar results.

Pairwise *t*-tests were then conducted to assess the significance of the observed differences in the prevalence of the different types of active deformation systems [34]. For a given pair of distinct experiments, each with five possible deformation systems, there were 25 possible comparisons. Since there are nine data sets (each row in Table 2), there are 36 possible distinct data set pairs (${}_9C_2$ i.e. 9!/7!/2!). With five different deformation systems in each data set to be compared, a total number of 900 possible comparisons of the relative activity of deformation systems can be considered. Moreover, with five deformation systems in each of the nine data sets, 20 distinct

Table 4. The *P value* associated with rejecting the hypothesis that the deformation system listed in a given row is *more likely* to be observed than that listed in the corresponding column. Negative numbers correspond to same probability of an error when a system in a given row is *less likely* to be observed than that in a given column.

		Ti–5Al–2.5Sn at 296 K and 3.5% Strain				
		Basal	Prismatic	Pyr ⟨a⟩	Pyr ⟨c+a⟩	Twin
CP Ti at 296 K and 4% Strain	Basal	−3.7E−11	−1.2E−15	0.0275	0.0544	0.0028
	Prismatic	0.00024	**0.0129**	1.4E−25	1.25E−24	4.08E−28
	Pyr <a>	−3E−16	−7.6E−22	0.219	0.342	0.0347
	Pyr <c+a>	−3.7E−11	−1.2E−15	0.0275	**0.0544**	0.00284
	Twin	−3.3E−10	−1.8E−14	0.0157	0.0323	0.00149

comparisons within each data set could also be made (omitting self-comparison). This results in an additional 180 potential tests, for 1080 total pairwise comparisons of the relative deformation system activity. Of these 1080 possible comparisons, 225 cases related to the observations mentioned above were investigated.

As an example of one of the 36 possible data set comparisons, Table 4 provides a listing of all the possible comparisons for the five types of deformation systems observed in CP Ti at 296 K and ~4% strain and the same deformation systems in Ti–5Al–2.5Sn at 296 K and ~3.5% strain. The number corresponding to a given row/column combination represents the probability of an error in asserting that the deformation mechanism listed in a given *row* is more likely than that listed in the related *column*. Negative numbers are the result of reversing the role of the column and row in the comparison. For example, the assertion that prismatic slip is more likely to be observed in CP Ti at ~4% strain and 296 K (row 1 in Table 2) than prismatic slip in Ti–5Al–2.5Sn at 3.5% strain and 296 K (row 6 in Table 2) has only 1.29% chance of being incorrect (bold number in row 2 column 2 in Table 4). Similarly, the assertion that pyramidal ⟨c + a⟩ slip is more likely to be observed at 296 K and ~4.3% strain in CP Ti, than pyramidal ⟨c + a⟩ slip at 296 K and ~3.5% strain in Ti–5Al–2.5Sn, has 5.44% chance of being an incorrect conclusion. This type of analysis allows the qualitative assessment of the relatively likelihood of the slip activity discussed in Sections 4.1–4.3, to be assigned a level of statistical confidence.

Thus, a number of statements can be supported by this statistical analysis. Note that in all of the conclusions below, the given *P-value* corresponds to the probability of making an error in rejecting the asserted hypothesis:

(1) In tensile tests of CP Ti, the activation of different slip systems is unaffected by the change in temperature from 296 to 728 K for similar strain level. Specifically, the probability of making an error in rejecting a hypothesis that temperature does affect the activity of different slip systems is at least 20% and can be as high as 50%, depending on which slip systems are being compared. ($0.20 \leqslant P \leqslant 0.50$).
(2) In tensile tests of Ti–5Al–2.5Sn, activation of different slip systems is also unaffected by a change in temperature. However, the likelihood of making an error with an assertion that temperature *is* important in Ti–5Al–2.5Sn is markedly

lower than in CP Ti, with the maximum error in Ti–5Al–2.5Sn no larger than 32.7% (pyramidal ⟨a⟩ slip) and as small as 12.4% (prismatic slip). The latter statistic indicates that prismatic slip is slightly favoured at low temperatures.

(3) At similar strain levels (~4.0% strain), the basal slip activity in Ti–5Al–2.5Sn was significantly more likely than in CP Ti at both 296 K ($P = 3.7 \times 10^{-11}$) and 728 K ($P = 2.8 \times 10^{-7}$).

(4) Twinning was more likely in CP Ti than in Ti–5Al–2.5Sn at similar strain levels (~4%) and at both 296 and 728 K (in all cases, $P \leqslant 0.0015$).

(5) Pyramidal ⟨c + a⟩ slip in CP Ti is more likely than pyramidal ⟨c + a⟩ slip in Ti–5Al–2.5Sn under similar strain and temperature conditions ($P \leqslant 0.054$).

(6) In CP Ti, for each individual data set, prismatic slip is by far the most likely slip system to activate at all temperatures and strain levels. The largest chance of making an error with this assertion occurs at ~4.3% strain and 728 K with $P = 1.2 \times 10^{-12}$.

(7) For sufficiently high Schmid factors, the data support the assertion that basal slip is preferred to prismatic slip in Ti–5Al–2.5Sn. Indeed, when the Schmid factor exceeds 0.35, the likelihood of making an error with such an assertion is no larger than 1.2%. However, when data including all possible Schmid factors are considered, any assertion that either basal or prismatic slip is preferred over the other in Ti–5Al–2.5Sn is more likely to be wrong ($P \geqslant 0.178$).

(8) In CP Ti at 728 K, the relative likelihood of basal, prismatic and pyramidal ⟨c + a⟩ slip systems being activated in tension at ~11.2% strain was indistinguishable from analogous activation likelihoods in creep at 45 MPa deformed to ~23.2% strain ($P \geqslant 0.181$). On the other hand, pyramidal ⟨a⟩ slip was significantly more likely during creep at ~23.2% strain than in tension at ~11.2% strain ($P = 0.0132$), and twinning was significantly more likely in tension at ~11.2% strain than in creep at ~23.2% strain ($p = 0.0119$).

(9) In Ti–5Al–2.5Sn at 728 K, the relative likelihood of pyramidal ⟨a⟩ and pyramidal ⟨c + a⟩ slip being activated in tension at ~9% strain was indistinguishable from analogous activation likelihoods in creep at 250 MPa with ~16.5% strain ($P \geqslant 0.179$). However, prismatic slip was significantly more likely in tension at ~9% strain than in creep at ~16.5% strain ($p = 1.27 \times 10^{-6}$). Further, basal slip in tension at ~9% strain is less prevalent than in creep at ~16.5% strain ($p = 6.2 \times 10^{-7}$).

(10) When comparing the relative activity of slip systems in CP Ti at 728 K undergoing creep at ~23.2% strain and Ti–5Al–2.5Sn undergoing creep at ~16.5% strain, prismatic ($p = 1.88 \times 10^{-12}$), pyramidal ⟨a⟩ ($p = 0.000633$) and pyramidal ⟨c + a⟩ slip ($p = 0.0807$) were all more likely in CP Ti than Ti–5Al–2.5Sn. On the other hand, basal slip was significantly more likely in Ti–5Al–2.5Sn than CP Ti during creep ($p = 7.5 \times 10^{-21}$).

5. Conclusions

The tensile deformation behaviour of CP Ti and Ti–5Al–2.5Sn was analysed and compared at both 296 and 728 K. Slip behaviour was assessed by observing instances of

surface slip visible in SEM images. Quantitative observations, augmented with rigorous statistical analysis, allowed several conclusions to be made. Prismatic slip was the most commonly observed deformation mode in both CP Ti and Ti–5Al–2.5Sn. Compared with CP Ti, basal slip activity was significantly enhanced in Ti–5Al–2.5Sn. This can be explained by the increased *c*/*a* ratio in Ti–5Al–2.5Sn. In general, when the global Schmid factor of prismatic slip exceeded 0.4, it was shown to be an effective parameter to predict the activation of prismatic slip for both CP Ti and Ti–5Al–2.5Sn. However, this was not the case for basal slip in CP Ti because prism slip was dominant, and it was activated at a much lower stress than in the alloy. Temperature did not significantly affect the relative activity of the tensile deformation modes in either material. In addition to dislocation slip, twinning was also an active deformation mode in CP Ti. However, it was almost completely suppressed in Ti–5Al–2.5Sn. Thus, alloying led to a more balanced amount of prismatic and basal slip activity, and it reduced $\langle c+a \rangle$ activity and suppressed twinning. Dislocation slip was the primary deformation mechanism in 728 K-45 MPa creep of CP Ti, while dislocation slip was observed to a significantly lesser extent during 728 K-250 MPa creep of Ti–5Al–2.5Sn, where GBS appeared to dominate.

Acknowledgements

This research was supported by the US Department of Energy, Office of Basic Energy Science through grant No. DE-FG02-09ER46637. The authors are grateful to Mr. James Seal and Mr. Zhe Chen of Michigan State University for their assistance with the sample preparation and *in-situ* tests. The authors are grateful to Thomas Van Daam of Pratt & Whitney, Rocketdyne for providing the Ti–5Al–2.5Sn alloy used in this study and Dr. Christopher Cowen, previously at National Energy Technology Laboratory, Albany, Oregon and currently at United States Mint, West Point, NY, who provided the CP Ti used in this study.

Note

1. Henceforth, all alloy compositions are given in weight percent.

References

[1] S. Nemat-Nasser, W.G. Guo and J.Y. Cheng, Acta Mater. 47 (1999) p.3705.
[2] A.A. Salem, S.R. Kalidindi, R.D. Doherty and S.L. Semiatin, Metall. Mater. Trans. A 37 (2006) p.259.
[3] Y. Yang, L. Wang, T.R. Bieler, P. Eisenlohr and M.A. Crimp, Metall. Mater. Trans. A 42A (2011) p.636.
[4] S. Zaefferer, Mater. Sci. Eng., A 344 (2003) p.20.
[5] W.H. Hosford, *The Mechanics of Crystals and Textures Polycrytals*, Oxford University Press, New York, NY, 1993.
[6] J.W. Christian and S. Mahajan, Prog. Mater Sci. 39 (1995) p.1.
[7] J. Gong and A.J. Wilkinson, Acta Mater. 57 (2009) p.5693.
[8] H. Conrad, Prog. Mater Sci. 26 (1981) p.123.
[9] A. Akhtar and E. Teghtsoonian, Metall. Mater. Trans 6A (1975) p.2201.
[10] F. Bridier, P. Villechaise and J. Mendez, Acta Mater. 53 (2005) p.555.
[11] J.C. Williams, R.G. Baggerly and N.E. Paton, Metall. Mater. Trans. A 33A (2002) p.837.
[12] D.G. Teer and F.B. Salem, Thin Solid Films 45 (1977) p.583.

[13] D. Buckley and R. Johnson, NASA Tech Note 1966; TN-D-3235.
[14] G. Lütjering and J.C. Williams, *Titanium*, Springer-Verlag, Berlin, 2003.
[15] L. Wang, Y. Yang, P. Eisenlohr, T.R. Bieler, M.A. Crimp and D.E. Mason, Metall. Mater. Trans. A 41 (2010) p.421.
[16] A. Akhtar, Metall. Mater. Trans. A 6A (1975) p.1105.
[17] N.E. Paton and W.A. Backofen, Metall. Trans. 1 (1970) p.2839.
[18] C.J. McHargue and J.P. Hammond, Acta Metall. 6 (1953) p.700.
[19] D.R. Chichili, K.T. Ramesh and K.T. Hemker, Acta Mater. 46 (1998) p.1025.
[20] N.E. Paton, J.C. Williams and G.P. Rauscher, The deformation of alpha-phase titanium, in *Titanium Science and Technology, Proceedings of the Second International Conference*, R.I. Jaffee and H.M. Burte, eds., Plenum Press, New York, NY, 1973.
[21] H. Li, C.J. Boehlert, T.R. Bieler and M.A. Crimp, Philos. Mag. 92 (2012) p.2923.
[22] ASTM. E112–96 Standard Test Methods for Determining Average Grain Size; 2004.
[23] J. Seal, M.A. Crimp, T.R. Bieler and C.J. Boehlert, Mater. Sci. Eng., A 552 (2012) p.61.
[24] R. Boyer, G. Welsch and E.W. Collings, *Materials Properties Handbook: Titanium Alloys*, ASM International, Materials Park, OH, 1994.
[25] A. Molinari, G.R. Canova and S. Ahzi, Acta Mater. 35 (1987) p.2983.
[26] A. Prakash and R.A. Lebensohn, Model. Simul. Mater. Sci. Eng. 17 (2009) p.064010.
[27] A.K. Kanjarla, P.V. Houtte and L. Delannay, Int. J. Plast. 26 (2010) p.1220.
[28] L. Wang, R.I. Barabash, Y. Yang, T.R. Bieler, M.A. Crimp, P. Eisenlohr, W. Liu and G.E. Ice, Metall. Mater. Trans. A 42A (2011) p.626.
[29] S.R. Kalidindi, A. Bhattacharyya and R.D. Doherty, Proc. R. Soc. Lond. A 49 (2004) p.1935.
[30] M.G. Zelin, H.S. Yang, R.Z. Valiev and A.K. Mukherjee, Metall. Mater. Trans. A 23A (1992) p.3135.
[31] T.G. Langdon, Philos. Mag. 22 (1970) p.689.
[32] A.H. Chokshi, J. Mater. Sci. 25 (1990) p.3221.
[33] R.G. Miller, Jr. *Beyond ANOVA Basics of Applied Statistics*, Chapman & Hall, New York, NY, 1998.
[34] C. Croarkin and P. Tobias, *NIST/SEMATECH e-Handbook of Statistical Methods*. [cited 2012 Apr]. Available at http://www.itl.nist.gov/div898/handbook/index.htm.